MODELING OF MULTIPHASE FLOW USING LEVEL SET METHOD AND ACCURATE HYPERBOLIC SOLVERS

Tamer KASEM[1] and Jun SASAKI[2]

[1]Graduate Student, M. Eng., Dept. of Civil Engineering, Yokohama National University (79-5 Tokiwadai, Hodogaya-ku, Yokohama 240-8501, Japan)

[2]Member of JSCE, D. Eng., Professor, Dept. of Civil Engineering, Yokohama National University (79-5 Tokiwadai, Hodogaya-ku, Yokohama 240-8501, Japan)

レベルセット法に基づく混相流モデリングではナビエ・ストークスソルバーと相境界の扱いの2点の選択が重要である．本研究では気液二相流を対象とし，ナビエ・ストークスソルバーとしてCCUP法を採用し，相境界の扱いについては，1～0の値を取るカラー関数で表現する方法と距離関数で表現する方法の2通りの場合について比較検討を行った．移流項の解法にはCIP-CSL3およびWENO5を採用し，上述の2通りの相境界の取り扱い法と組み合わせた，計4通りの手法をダムブレーク問題に適用することで，それぞれの性能について比較検討を行った．その結果，これらの中ではWENO5と距離関数を組み合わせた方法が総合的に見て最も優れていることが明らかとなった．本手法を気液二相流におけるソリトン波に適用し，その有効性を検証した．

Key Words : *Level Set, Free surface flow, CCUP, CFD, WENO, CIP-CSL3*

1. INTRODUCTION

Simulation of multi-phase flow problems is an important topic in modern research. In such problems two immiscible fluids of different phases (liquid and gas) are present in the problem domain. A typical example for such problems is modeling of surface water waves. Boundary layer methods were applied widely for such problems[1)]. However in CFD methods, the fluid governing equations are solved numerically and viscous effects are applied directly to the whole domain. Constraints due to perturbation parameters present in boundary layer methods are absent in CFD. Numerical solution of flow equations demands determination of gas-liquid interface location (curve in 2-D and surface in 3-D), to provide fluid properties. Two methods are mentioned extensively in the literature for doing such task; VOF and level set. A disadvantage of VOF is the discontinuity in gas-liquid interface between computation cells[2)]. Also in VOF careful calculation of mass flux across cell boundaries is needed[3)]. The absence of such step in level set method makes it simpler. The present work adopts the level set method. In the level set method, the computation algorithm is broken into two main blocks. Upon substituting the fluid properties in Navier-Stokes solver block (NSB), the fluid velocities are obtained, and the gas-liquid interface location is updated in the fluid interface block (FIB). Such cycle is illustrated in **Fig. 1**.

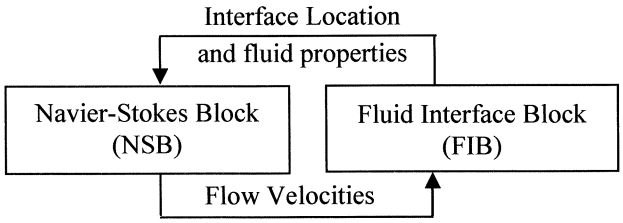

Fig. 1 Main blocks and main cycle of level set method

Upon designing FIB, two decisions should be taken; the form of the color function ϕ used to present liquid-gas regions, and the method for advancing ϕ in time. One possible form of ϕ, is assigning it a value of one and zero in liquid and gas regions respectively (ϕ_{1-0}). Another form is assigning ϕ to the distance from the interface (ϕ_d). Both forms are compared in **Fig. 2** where a liquid drop surrounded by gas is illustrated.

Both ϕ_{1-0} and ϕ_d are advanced in time by solving an advection equation. Two candidate

methods for that task are a CIP type or an ENO type solver. In the current literature ϕ_{1-0} is always used with a CIP type solver[4), 5), 6)]. On the other hand ENO type solvers are always used with ϕ_d[7), 8), 9)]. In the present work the reason of such coupling is clarified. Also different configurations are compared to reveal their advantages.

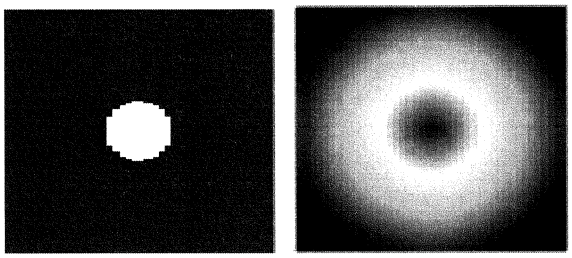

Fig. 2 Representation of a liquid drop surrounded by a gas, left is ϕ_{1-0} and right is ϕ_d.

2. COMPARISON OF ϕ_d AND ϕ_{1-0}

In the present section both presentations (ϕ_{1-0} and ϕ_d) are detailed. Since ϕ is advected passively with the fluid, both presentations are integrated in time using Eq. (1).

$$\frac{\partial \phi}{\partial t} + \nabla \cdot (\underline{V}\phi) = 0 \tag{1}$$

For an incompressible fluid, fluid properties of interest are the density ρ and the viscosity μ. For both presentations fluid properties are calculated using Eq. (2):

$$\begin{aligned} \rho &= \rho_L \phi_{comp} + \rho_G (1 - \phi_{comp}) \\ \mu &= \mu_L \phi_{comp} + \mu_G (1 - \phi_{comp}) \end{aligned} \tag{2}$$

where μ_L, ρ_L, μ_G and μ_L are dynamic viscosities and densities of liquid and gas respectively. ϕ_{comp} is computed using Eq.(3).

$$\phi_{comp} = \begin{cases} 0 & \text{if } \phi_{1-0} < \epsilon \\ 1 & \text{if } \phi_{1-0} > 1 - \epsilon \\ \phi_{1-0} & \text{else} \end{cases} \tag{3a}$$

$$\phi_{comp} = \begin{cases} 0 & \text{if } \phi_d < -\delta \\ 1 & \text{if } \phi_d > \delta \\ 0.5\left(1 + \sin\left(\frac{\pi \phi_d}{2\delta}\right)\right) & \text{else} \end{cases} \tag{3b}$$

Eq.(3a) is used if ϕ_{1-0} is adopted while Eq.(3b) is used if ϕ_d is adopted[7)]. ϵ is an arbitrarily small parameter selected as 0.05 in the present work. On the other hand δ is calculated from Eq.(4) using Δ the grid size[7)]:

$$\delta = \frac{\phi_{max} - \phi_{min}}{2} = 1.5\Delta \tag{4}$$

Fig. 3 illustrates both formulations near the gas-liquid interface. Considering **Fig. 3**, Eq.(2), (3) and (4) the following notes should be mentioned.

A major drawback of ϕ_{1-0} presentation is the uncontrolled thickness of the gas-liquid interface region. Due to the sharp transition from 0 to 1, such thickness should not exceed Δ . However such width cannot be achieved in practice due to numerical errors upon solving Eq.(1). On the other hand when ϕ_d is used, Eq.(5) is solved (re-initialization), after Eq.(1).

$$\frac{\partial \phi_d}{\partial \tau} = \text{sign}(\phi_d)(1 - |\nabla \phi_d|) - \frac{\int_{\Omega_{ij}} H'(\phi_d) \frac{\partial \phi_d}{\partial t}}{\int_{\Omega_{ij}} H'(\phi_d) f(\phi_d)} H'(\phi_d) |\nabla \phi_d| \tag{5}$$

Definition of terms appearing in Eq.(5) (H', Ω_{ij}, etc.) and solution steps are omitted due to space limits, however full details are provided by Sussman[8)]. Solving Eq.(5) consumes extra time, but assures that the slope of ϕ_d is kept equal to unity. Also careful re-initialization does not change the interface place (intersection between ϕ_d and zero level) and ensures mass conservation.

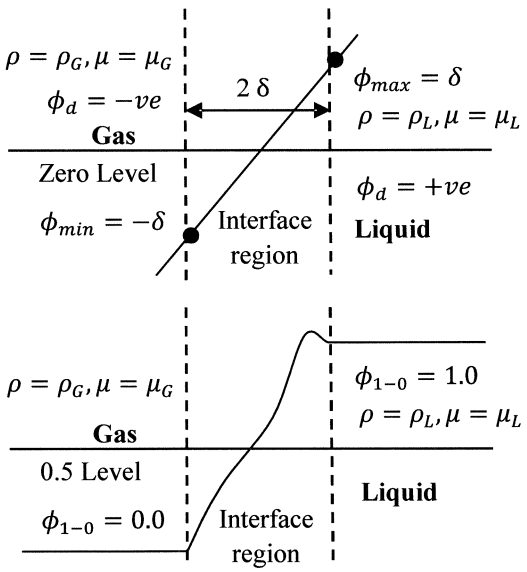

Fig. 3 Typical form of ϕ_d (up) and ϕ_{1-0} (down) near the gas liquid interface.

3. COMPARISON OF CIP AND ENO SOLVERS

(1) CIP solvers (CIP-CSL3)

The goal of using a CIP or an ENO type method is solving Eq.(1) accurately. Providing a full review of various CIP type methods is beyond the scope of

the current work. However CIP-CSL3 method is selected as a typical example of such solvers. Following the pioneer work where the original version of CIP method[10] was introduced, the enhanced version CIP-CSL3[11] was suggested and widely applied[5), 6), 11), 12)].

The logic of CIP-CSL3 method is based on splitting Eq.(1) into two phases

$$\frac{\partial \tilde{\phi}}{\partial t} + \underline{V} \cdot \left(\nabla \tilde{\phi}\right) = 0 \tag{6a}$$

$$\frac{\partial \phi}{\partial t} + \tilde{\phi}\left(\nabla \cdot \underline{V}\right) = 0 \tag{6b}$$

Using the method of characteristics, Eq.(6a) is solved as:

$$\begin{aligned} \tilde{\phi}\left(\underline{X}, t\right) &= \phi\left(\underline{X} - \underline{V}\Delta t, t - \Delta t\right) \\ &= \phi^{n-1}\left(\underline{X} - \underline{V}\Delta t\right) \end{aligned} \tag{7}$$

The Lagrangian solution at t ($\tilde{\phi}$) is obtained from the old solution (at $t - \Delta t$) by direct substitution. After $\tilde{\phi}$ is obtained, the new solution ϕ (at t) is obtained from Eq.(6b) by explicit finite difference. The main difficulty in such concept is the need of adequate interpolation of the space profile of ϕ^{n-1}. For a discontinuous profile, interpolation using polynomials leads to spurious oscillations (Gibbs phenomena[13]). In CIP-CSL3 a cubic spline is used for interpolation. Compared to the original CIP method[10], the fictitious oscillations are much reduced in CIP-CSL3. Also partial derivatives are not included.

The CIP-CSL3 method is based on a one-dimensional (1D) subroutine where two vectors are updated. The two vectors are $\phi_{i-1/2}$ and $\overline{\phi}_i$, which are respectively the function value at the left boundary and the function average at cell i. Undesired oscillations are reduced by careful choice of the space derivative at the cell center. Extension to two-dimensions (2D) is achieved by applying the 1D procedure sequentially in alternating directions. In two dimensions the function value is no longer used at the cell boundaries. Instead $\phi_{i-1/2,j}$ is defined as the surface average at the left face of cell i, j. Upon applying the 1D algorithm in one direction, the face averages in the other direction are not updated. Such difficulty is treated by using the TEC equation[12], where surface average values are updated using cell average values. The full details of CIP-CSL3 method is found in Xiao[11].

(2) ENO solvers (WENO5)

In ENO type methods, The flux term in Eq.(1) $(\nabla \cdot (\underline{V}\phi))$ is discretized by interpolation of $\underline{V}\phi$. Such interpolation is done using a weighted sum of all possible Lagrangain polynomials[13]. The weights are selected to decrease the undesired oscillations. Among the various ENO methods, WENO5 is selected as a typical example in the current work.

In WENO5 method three 3rd order Lagrange polynomials are summed. The resulting scheme is 5th order space accurate. Special care is needed to obtain correct entropy solutions. Depending on local velocity values, up-winding, down-winding or flux splitting is used[14]. Time integration of Eq.(1) can be done with different schemes. In the present work integration is done using forward Euler explicit method. For a comprehensive discussion about ENO methods and a detailed description of WENO5 method the reader may consult Shu[14].

(3) CIP-CSL3 versus WENO5

Here we compare between the performance of CIP-CSL3 and WENO5. In addition to the function values required in WENO5, the function volume and surface average are required in CIP-CSL3. Such requirements need extra memory and complicate analysis. Another advantage of WENO5 over CIP-CSL3 is the relatively simple extension to multi-dimensions.

The semi-Lagrangian concept of the CIP-CSL3 method is straightforward to program and understand. The relatively complicated process of flux splitting required in WENO5 is absent in CIP-CSL3. However the semi-Lagrangian concept complicates application of CIP-CSL3 to hyperbolic equations with a source term at the right hand side like Eq.(5). It is not a trivial task to do re-initialization using CIP-CSL3. The authors believe that, this is the reason why CIP-CSL3 is always used with ϕ_{1-0} where no re-initialization is needed. In the present work ϕ_d is used with CIP-CSL3. Eq.(5) is solved separately with the method described in Sussman[8]. In order to maintain consistency, the solution of Eq.(5) is substituted into TEC formula and the surface values used in CIP-CSL3 are updated.

4. RESULTS AND DISCUSSION

(1) Verification and comparison

In the next section results from applying different choices are shown. Three combinations are presented, ϕ_{1-0} with CIP-CSL3 (CSL3-SHRP), ϕ_d with WENO5 (WENO-DST) and finally ϕ_d with CIP-CSL3 (CSL3-DST). CSL3-SHRP and WENO-DST were applied widely[5),6),15),16)]. A new option examined in the present study is CSL3-DST. In all cases CCUP method[17] is used to solve the incompressible flow equations in Navier-Stokes

solver block. The three options are tested against the benchmark dam-break problem.

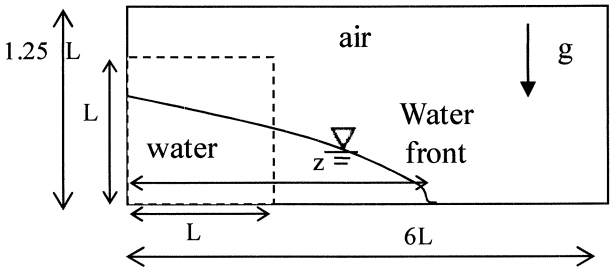

Fig. 4 Dam break problem configuration

In the dam break problem a column of water is initially held behind a barrier. The barrier is suddenly removed and the water column collapses and flows under gravity (see **Fig. 4**). No slip boundary conditions are applied at left and lower boundaries. For right and upper boundaries, extrapolation boundary conditions are applied to the velocities. Such problem depends on the following parameters:

$R_e = V_\infty \rho_w / v_w$, $\mu_{rat} = \mu_w / \mu_g$, $\rho_{rat} = \rho_w / \rho_g$,

where R_e , μ_{rat} and ρ_{rat} are the Reynolds number and water gas viscosity and density ratios, respectively. The characteristic velocity V_∞ is given by $\sqrt{2gL}$. The characteristic length and time are taken as L and $\sqrt{L/(2g)}$, respectively.

The problem is calculated for two cases. For both cases $\mu_{rat} = 56.04$ and $\rho_{rat} = 831.7$. While for case 1 and case 2 R_e is equated to 6×10^4 and 1.43×10^5, respectively. The values are taken to be consistent with the experiment done by Martin[18]. Although such measurements are old, they are still used for validation by modern works[6)19)].

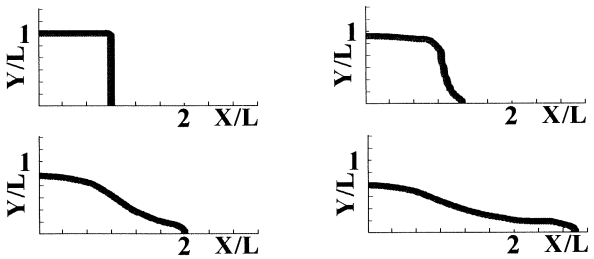

Fig. 5 Free surface profile, WENO-DST, case 1, t =0,1,2,3.

In **Fig. 5** a typical simulated free surface profile is shown is shown. **Fig. 6** shows the calculations by the three combinations against measurements (water front location). An equidistant Cartesian grid is used. Grid size is 150×125 divisions in the horizontal and vertical directions respectively. 20,000 and 25,000 time steps are used to reach $t_{max} = 4.0$ for case 1 and case 2, respectively. For case 1, deviation between simulation and measurements increases with time. For case 2, the agreement between simulation and measurement is better. The same observation was made by Kelecy[20].

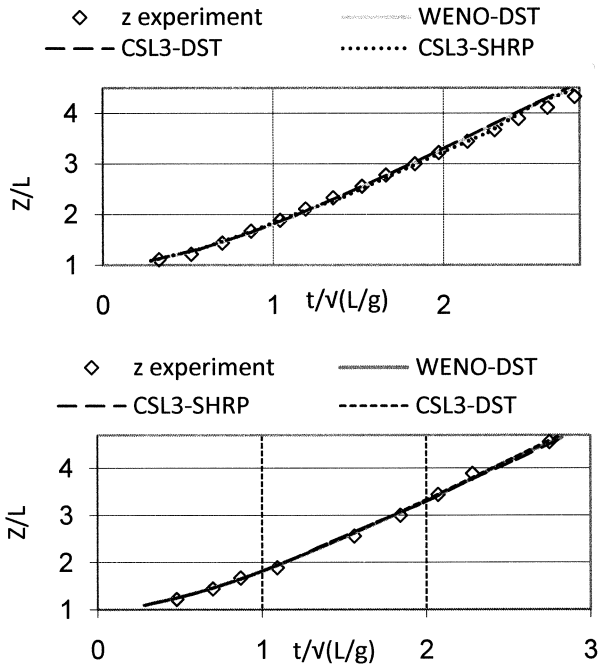

Fig. 6 Front Position versus time. Up is case 1, Down is case 2.

Free surface profile at $t = 4$ for case 1 is shown in **Fig. 7**. The surface profile is marked by the value of ϕ_{comp}=0.5. The contour plots extend from ϕ_{comp}=0.05 to 0.95.

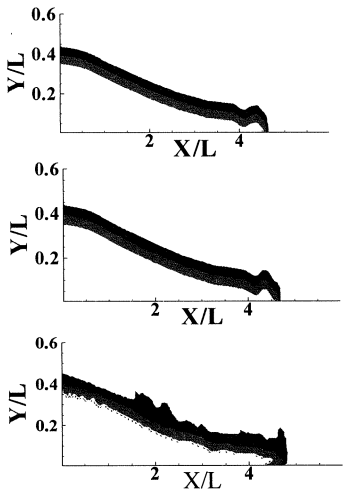

Fig. 7 Free surface profile at t=4. Top to bottom is WENO-DST, CSL3-DST and CSL3-SHRP.

The Three combinations yield very close results in terms of the front position (see **Fig. 6**). However the surface profile resulting from CSL3-SHRP is relatively irregular.

It is clear from the present section that ϕ_d has a valuable advantage against ϕ_{1-0}. We also note that

the computation time for the three methods were comparable. Mentioning the complications of CSL3-DST compared to WENO-DST (extra data structures and difficulty in treating source terms) WENO-DST should be regarded as the optimum choice. It is also clear that the performance of CCUP with the different choices is satisfactory. We note that other Navier-Stokes solvers were successfully combined with WENO[15),16)]. It is concluded that the internal details of NSB may be independent on those of the FIB.

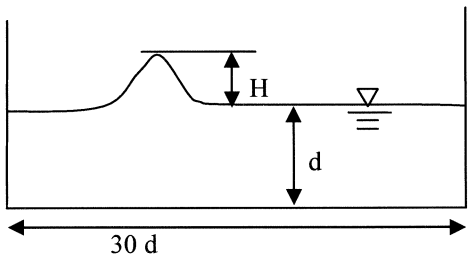

Fig. 8 Solitary wave problem definition

(2) Simulation of Solitary Wave Propagation

To further illustrate the ability of WENO-DST Solitary wave propagation is simulated. The problem setup (see **Fig. 8**) is the same as Hu[4)] and Tang[21)].

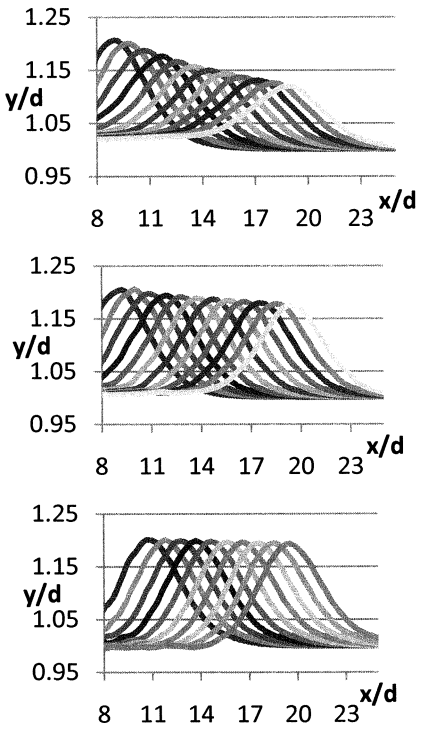

Fig. 9 Free surface profile at different times for Re =50, 500 and 50000 (top to bottom)

In addition to the following already defined parameters, R_e, μ_{rat} and ρ_{rat}, the problem depends also on H/d, dimensionless wave height. The characteristic velocity is calculated as $V_\infty = \sqrt{gd}$. The characteristic length and time are taken as d and $\sqrt{d/g}$, respectively. Simulation is done for $\mu_{rat} = 50.6$, $\rho_{rat} = 831.7, H/d$ =0.2 and three values of R_e; 50, 500 and 50,000. The wave peak is initiated at $x = 8d$. The simulation is run up to $t = 10.5$, with total of 6000 time steps. Grid size is 180×30 divisions in the horizontal and vertical directions respectively.

Fig. 9 shows the surface profile at 10 equidistant time intervals, from step 2500 to 6000. **Fig. 10** shows the wave amplitude attenuation versus time. Both theoretical results[1)] and current model numerical results are shown. Numerical simulation includes damping due to bottom friction and air drag over the wave profile, while theoretical formula includes only bottom boundary layer effect. That is why attenuation rate from simulation is higher than attenuation by theoretical formula of Mei[1)]. Such result agrees with previous works[4),21)]. Also the difference between theoretical and numerical results decreases as R_e increases. That is expected since the boundary layer approximation becomes more valid for high R_e.

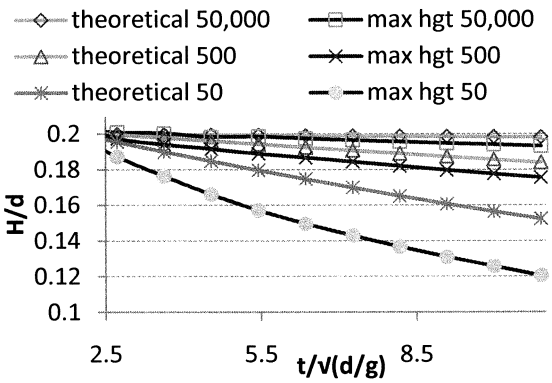

Fig. 10 Wave amplitude versus time

Water of depth 1 m, yields $R_e = 3.1 \times 10^6$, which is a relatively practical value. For such case velocity vectors near the interface is plotted for different values of H/d (see **Fig. 11**). The three plots shed light on the mechanism of momentum transfer from water to air. As the wave propagates from left to right, the air is pushed by the wave front. However due to continuity of velocity at the interface, air follows the wave back at the left. Such motion induces an air vortex over the wave crest. The vortex size and strength increase as the wave height increases. The result from the present section illustrates the advantage of CFD methods over boundary layer solutions where air dynamics is totally neglected.

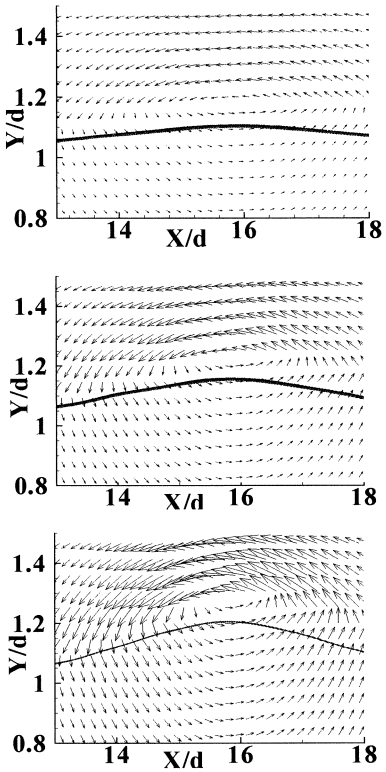

Fig. 11 Velocity vectors near free surface for H/d = 0.1, 0.15 and 0.2 (top to bottom) at $R_e = 3.1 \times 10^6$

5. CONCLUSIONS

Different configurations of the FIB in the level set method are explored. Models are verified against dam break benchmark problem. Although different configurations results are satisfactory, considering regular profile and simple data structures, the optimum choice is WENO-DST. The proposed choice is used to simulate the propagation of a solitary wave. The results obtained are consistent with past works and theory. Moreover the details of multiphase flow near the air water interface are revealed for different cases. A powerful extension of the present model in the future is accounting for irregular topography and turbulence. With those extensions the details of wave deformation and breaking due to variable topography and engineering structures can be revealed, providing essential data for civil design engineers.

ACKNOWLEDGMENT: The present study is partially funded by JSPS Grant in Aid for Scientific Research (B) (No. 15360263).

REFERENCES

1) Mei, C.: *The applied dynamics of ocean surface waves, Advanced series in ocean engineering, Volume 1*, World Scientific, 1994.
2) Losasso, F., Fedkiw, R. and Osher, S.: Spatially adaptive techniques for level set methods and incompressible flow, *Comput. Fluids*, Vol.35, pp.995-1010, 2006.
3) Hirt, W., and Nichols, D.: Volume of fluid (vof) method for the dynamics of free boundaries, *J. Comput. Phys.*, Vol.39, pp.201-225, 1981.
4) Hu, C. and Kashiwagi, M.: A cip-based method for numerical simulations of violent free-surface flows, *J. Mar. Sci. Technol.*, Vol.9, pp.143-157, 2004.
5) Kishev, Z., Hu, C. and Kashiwagi, M.: Numerical simulation of violent sloshing by a cip-based method, *J. Mar. Sci. Technol.*, Vol.11, pp.111-122, 2006.
6) Xiao, F. and Ikebeta, A.: An efficient method for capturing free boundaries in multi-fluid simulations, *Int. J. Num methods Fluids*, Vol.42, pp.187-210, 2003.
7) Sussman, M., Smereka, P. and Osher, S.: A level set approach for computing solutions to incompressible two-phase flow, *J. Comput. Phys.*, Vol.114, pp.146-159, 1994.
8) Sussman, M. and Fatemi, E.: An efficient, interface-preserving level set redistancing algorithm and its application to interfacial incompressible fluid flow, *SIAM J. Sci. Comput.*, Vol.20, pp.1165-1191, 1999.
9) Chang, Y., Hou, T., Merriman, B. and Osher, S.: A level set formulation of eulerian interface capturing methods for incompressible fluid flows, *J. Comput. Phys.*, Vol.124, pp. 449-464, 1996.
10) Takewaki, H., Nishiguchi, A., and Yabe, T.: The cubic-interpolated pseudo-particle (cip) method for solving hyperbolic type equations, *J. Comput. Phys.*, Vol.61, pp.261-268, 1985.
11) Xiao, F. and Yabe, T.: Completely conservative and oscillationless semi-lagrangian schemes for advection transportation, *J. Comput. Phys.*, Vol.170, pp.498-522, 2001.
12) Xiao, F., Ikebeta, A. and Hasegawa, T.: Numerical simulations of free-interface fluids by a multi-integrated moment method, *Computers and Structures*, Vol.83, pp.409-423, 2005.
13) Shu, C.-W.: Essentially non-oscillatory and weighted essentially non-oscillatory schemes for hyperbolic conservation laws, *Lecture Notes in Mathematics*, Vol.1697, pp.325-432, 1998.
14) Shu, C.-W. and Osher, S.: Efficient implementation of essentially non-oscillatory shock-capturing schemes, II, *J. Comput. Phys.*, Vol.83, pp.32-78, 1989.
15) Kang, M., Fedkiw, R., and Liu, X.: A boundary condition capturing method for multiphase incompressible flow, *J. Sci. Comp.*, Vol.15, pp. 323-360, 2000.
16) Tanguy, S. and Berlemont, A.: Application of a level set method for simulation of droplet collisions, *Int. J. Multiphase Flow*, Vol.31, pp.1015-1035, 2005.
17) Yoon, S. and Yabe, T.: The unified simulation for incompressible and compressible flow by the predictor-corrector scheme based on the cip method, *Comput. Phys. Commun.*, Vol.119, pp.149-158, 1999.
18) Martin, J. and Moyce, W.: An experimental study of the collapse of liquid columns on a rigid horizontal plane, *Phil. Trans. Royal Society London, Ser. A*, Vol.244, pp.312-324, 1952.
19) Marchandise, E., Remacle, J.: A stabilized finite element method using a discontinuous level set approach for solving two phase incompressible flows, *J. Comput. Phys*, Vol.219, pp.780–800, 2006.
20) Kelecy, F. and Pletcher, R.: The development of a free surface capturing approach for multidimensional free surface flows in closed containers, *J. Comput. Phys.*, Vol.138, pp.939-980, 1997.
21) Tang, C., Patel, V., and Landweber, L.: Viscous effects and reflection of solitary waves in shallow channels, *J. Comput. Phys.*, Vol.88, pp.86-113, 1990.